PERGAMON

International Journal of Impact Engineering 27 (2002) 19–35

INTERNATIONAL JOURNAL OF IMPACT ENGINEERING

www.elsevier.com/locate/ijimpeng

Perforation of 12 mm thick steel plates by 20 mm diameter projectiles with flat, hemispherical and conical noses Part I: Experimental study

T. Børvik*, M. Langseth, O.S. Hopperstad, K.A. Malo

Structural Impact Laboratory (SIMLab), Department of Structural Engineering, Norwegian University of Science and Technology, N-7491 Trondheim, Norway

Received 20 September 2000; received in revised form 16 February 2001; accepted 29 June 2001

Abstract

Projectiles with three different nose shapes (blunt, hemispherical and conical) have been used in gas gun experiments to penetrate 12 mm thick Weldox 460 E steel plates. Based on the experimental results, the residual velocity curves of the target material were constructed and compared. It was found that the nose shape of the projectile significantly affected both the energy absorption mechanism and the failure mode of the target during penetration. The ballistic limit velocities were about equal and close to 300 m/s for hemispherical and conical projectiles, while it was considerably lower for blunt projectiles. Blunt projectiles caused failure by plugging, which is dominated by shear banding, while hemispherical and conical projectiles penetrated the target mainly by pushing the material in front of the projectile aside. Also, the residual velocity curves were influenced by nose shape, partly due to the differences in projectile deformation at impact. The experimental study, given in this part of the paper forms the basis for explicit finite element analysis using the commercial code LS-DYNA presented in Part II of the paper. © 2001 Published by Elsevier Science Ltd.

Keywords: Penetration; Experiments; Nose shape; Energy absorption; Failure modes; Ballistic limit velocity

1. Introduction

Structural impact is known as a complex problem, both from an experimental, analytical and numerical point of view [1–3]. One reason is the many physical parameters involved that may cause highly non-linear and sometimes unexpected structural behaviour when varied. As an

*Corresponding author. Tel.: +47-73-59-46-47; fax: +47-73-59-47-01.
E-mail address: tore.borvik@bygg.ntnu.no (T. Børvik).

0734-743X/02/$ - see front matter © 2001 Published by Elsevier Science Ltd.
PII: S0734-743X(01)00034-3

Nomenclature

ΔD	projectile nose deformation, i.e. $\Delta D = D_f - D_i$
Δh_t	plug thinning, i.e. $\Delta h_t = h_t - h_{pl}$
ΔL	projectile length reduction, i.e. $\Delta L = L_i - L_f$
ΔK	change in kinetic energy
d	diameter
D	projectile nose diameter
h	thickness
HRC	hardness Rockwell C
K	kinetic energy
L	projectile length
m	mass
T	temperature
t	time
v	velocity
w	deformation
W	work

Subscripts

bl	ballistic limit
c	cavity
f	final value, fracture or front side
g	global part of target
i	initial value
l	local part of target
m	maximum value
p	projectile
pe	permanent value
pl	plug
r	residual value, rear side
t	target

example, Baker et al. [4] identified nearly 30 possible and relevant input parameters in the general penetration problem of metal plates. However, several of these parameters are problem-dependent and can be neglected in certain situations. One typical problem where the number of variables is limited is impact loading of stationary targets by explosion-generated fragments at sub-ordnance velocities. In this problem, it is assumed that the nose shape of hard projectiles severely affects the response of the target structure. Here, blunt projectiles normally cause failure by shear plugging, conical projectiles tend to give petaling in thin plates and ductile hole enlargement in thicker plates, while hemispherical projectiles seem to give failure by tensile stretching after severe indentation and thinning of the target plate. However, as pointed out by Woodward [5], in

many cases mixed modes of failure appear as a result of anisotropy in the target material at fracture.

Some investigations have studied as to what way different nose shapes affect the ballistic behaviour of the target material, but the results are to some extent incompatible. Experimental results by Grabarek presented in [6] indicated that the more blunt the nose shape is, the higher is the ballistic limit velocity. This is in some conflict with the results by Corran et al. [7], which showed that the critical impact energy depends on the projectile nose radius. They found that the energy reached a maximum when there was a change in failure mode from shear plugging to tensile stretching. Johnson et al. [8] reported similar results in quasi-static punching tests of metal plates. Ipson and Recht [9] found that sharp projectiles penetrated the target in a less efficient way than blunt projectiles, giving a higher ballistic limit for conical projectiles as long as the target thickness was moderate. However, for thin and thick targets conical projectiles were found superior. Wingrove [10] observed similar behaviour in perforation tests of 2014-T6 aluminium alloy targets. He showed that blunt projectiles penetrated the target with the least resistance, followed by hemispherical and ogive penetrators in that order, as long as the target thickness to projectile diameter ratio was less than one. Othe et al. [11] found that the critical perforation energies for blunt and hemispherical projectiles were similar, while less energy was required for conical projectiles. They also found a distinct drop in the perforation resistance of the target as the nose angle of the sharp projectile was decreased. This decrease in critical energy was attributed to the decrease in the effective contact area for the projectiles. Wilkins [12] found that sharp projectiles gave lower ballistic limits than blunt projectiles when fired into thick metal plates, while the opposite was found for thin targets.

The above and similar contradictions found in the literature indicate that the influence of projectile nose shape in structural impact is controlled by parameters varying from one investigation to the other. It follows that the problem is not yet fully solved, and more work is necessary in order to determine the governing variables of the problem. To this end, a study on the penetration of steel plates by projectiles with different nose shapes has been completed. The investigation is divided into two parts. In Part I, presented in this paper, three different projectile nose shapes (blunt, hemispherical and conical) are used in compressed gas gun experiments to penetrate 12 mm thick Weldox 460 E steel plates. The tests are carried out in order to study the importance of projectile nose shape in structural impact at sub-ordnance velocities, and to provide high-precision experimental data for validation of numerical computations. Based on the experimental results, the residual velocity curves of the target plates are constructed and compared, and the obtained differences in energy absorption and failure mode caused by varying the projectile nose shape are discussed in some detail. Numerical results from explicit finite element analysis of the problem are presented in Part II of the paper, see [13].

2. Experimental set-up and programme

The experimental programme on the ballistic penetration of 12 mm thick Weldox 460 E steel plates by projectiles with different nose shapes was carried out in the compressed gas gun shown in Fig. 1 [14]. In the tests, the sabot-mounted projectiles were fired at impact velocities just below and well above the ballistic limit of the target plate. The serrated sabot separated immediately

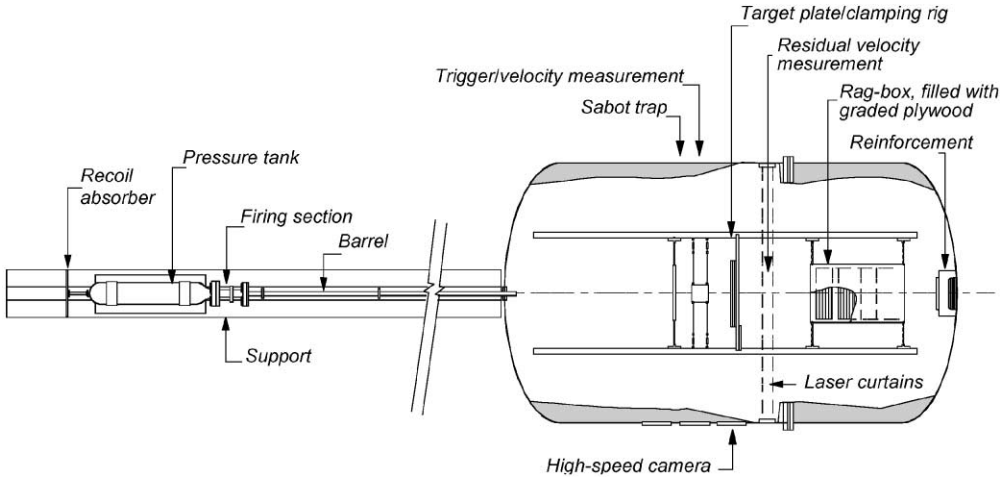

Fig. 1. Sketch of compressed gas gun used in the tests [14].

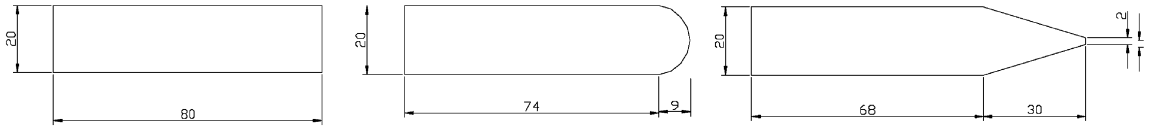

(a) (b) (c)

Fig. 2. The different projectiles used in the tests; (a) blunt, (b) hemispherical, (c) conical.

after leaving the muzzle due to aerodynamic forces, and the sabot pieces were stopped in a sabot trap prior to impact.

Projectiles were manufactured from Arne tool steel. After machining, they were oil hardened to a maximum Rockwell C value of 53 in order to minimise the plastic deformation during impact. Nominal hardness (HRC 53), diameter (20 mm) and mass (0.197 kg) of the cylindrical projectiles were constant in all tests. The L/D-ratio of the projectiles varied somewhat due to the constant mass. The geometry of the different projectiles used in the tests is defined in Fig. 2. Note that the tip of the conical projectile was removed, giving it a truncated cylindro-conical shape. Before testing, the projectiles were painted dead black and equipped with fiducial marks required for high-speed camera measurements [14,15].

The target plates, having a free span diameter of 500 mm and a constant nominal thickness of 12 mm, were clamped in a circular frame approximately 2 m behind the muzzle by 21 prestressed M16 bolts. In order to allow high-speed photography during penetration and perforation, the frame was equipped with a 150 mm framing window. All target plates were carefully sandblasted on both sides prior to testing. Target thickness, oblique, initial imperfections and final deformations were measured in situ. If perforation occurred, the projectile and possible plug were soft recovered in a rag-box filled with graded plywood.

Initial and final velocities were measured using different laser-based optical devices, and a digital high-speed camera system was used in all tests to photograph the penetration event. From

the digital images, impact angles and projectile velocities during penetration were determined using image processing. It is referred to [14,15] for further details regarding the experimental set-up and measurement techniques used in the penetration tests. The tensile material test results for the projectile and target have been presented elsewhere [15], but are also given in Part II of this paper [13].

3. Experimental results and discussion

Experimental results from 24 full-scale tests with blunt, hemispherical and conical nosed projectiles are given in Tables 1–3, respectively. The experimental data for blunt projectiles has partly been presented before [15], and is therefore mainly given for comparison. Based on the measured initial and residual velocities of the free-flying projectiles, the residual velocity curves in Fig. 3 were constructed. The ballistic limit velocities were calculated as the average between the highest impact velocity not giving perforation and the lowest impact velocity giving complete perforation of the target. The solid lines through the data points shown in Fig. 3 were fitted to an analytical model originally proposed by Recht and Ipson (1963)

$$v_{\mathrm{r}} = a(v_i^p - v_{\mathrm{bl}}^p)^{1/p}, \quad a = \frac{m_{\mathrm{p}}}{m_{\mathrm{pl}} + m_{\mathrm{p}}}, \quad p = 2. \tag{1}$$

Here, the method of least squares was used to find a best fit of the model constants a and p to the experimental values. The ballistic limit velocities obtained experimentally and the fitted values of a and p are given in Table 4.

From the residual velocity curves in Fig. 3 some immediate conclusions can be drawn. First, it is seen that the nose shape of the projectile significantly affects the ballistic resistance of the target plate. The ballistic limit velocities for hemispherical and conical projectiles are about equal and close to 300 m/s, while the ballistic limit velocity is as low as 185 m/s for blunt projectiles. The

Table 1
Experimental results with blunt projectiles

Test #	v_{i} (m/s)	v_{r} (m/s)	v_{rpl} (m/s)	m_{pl} (g)	$w_{\max}$ (mm)	d_{cf} (mm)	d_{cr} (mm)	ΔD (mm)	ΔL (mm)	t_{f}[b] (μs)
B20[a]	399.6	291.3	—	36.0	0.62	22.69	23.82	—	—	—
B1	303.5	199.7	242.3	27.6	1.01	20.65	20.93	1.01	0.90	60
B3	285.4	181.1	224.7	27.6	1.22	20.59	20.75	0.77	0.72	65
B2	244.2	132.6	187.7	28.1	1.22	20.42	21.18	0.50	0.53	69
B9	224.7	113.7	169.0	27.3	1.72	20.56	20.72	0.49	0.47	100
B4	200.4	71.4	103.7	27.8	2.08	20.35	20.88	0.29	0.28	104
B15	189.6	42.0	64.0	27.7	2.06	20.34	20.63	0.19	0.22	106
B14	184.3	30.8	45.3	27.8	2.04	20.35	20.64	0.17	0.20	110
B16	184.8	0	0	—	2.59	20.20	—	0.17	0.22	—
B8	181.5	0	0	—	2.92	20.21	—	0.11	0.24	—

[a] Projectile nose broke at impact.
[b] Estimated from the high-speed camera images.

Table 2
Experimental results with hemispherical projectiles

Test #	v_i (m/s)	v_r (m/s)	v_{rpl} (m/s)	m_{pl} (g)	w_{max} (mm)	d_{cf} (mm)	d_{cr} (mm)	ΔD (mm)	ΔL (mm)	t_f (μs)
H6	452.0	325.1	348.0	15.12	0.89	20.03	19.65	0.40	0.50	62
H7	420.6	284.3	301.8	19.80	1.43	21.16	20.17	0.22	2.38	84
H3	362.9	220.2	265.1	16.72	1.35	20.14	19.76	0.02	0.35	90
H5	326.7	154.8	189.4	18.08	1.97	20.1	19.68	0.01	0.33	102
H1	300.0	97.2	159.5	20.30	2.46	20.28	19.85	0.01	0.18	135
H4	292.1[a]	0	—	18.58	3.10	20.13	—	—	—	143
H2	278.9	0	—	—	—	—	—	—	—	—

[a] Assumed ballistic limit, see Fig. 6h.

Table 3
Experimental results with conical projectiles

Test #	v_i (m/s)	v_r (m/s)	v_{rpl} (m/s)	m_{pl} (g)	w_{max} (mm)	d_{cf} (mm)	d_{cr} (mm)	ΔD (mm)	ΔL (mm)	t_f[a] (μs)
C7	405.7	312.0	—	—	1.73	20.82	19.61	0.01	0.19	46
C4	355.6	232.3	—	—	1.95	20.58	19.59	0.02	0.05	52
C2	317.9	155.8	—	—	2.83	20.19	19.76	0.02	0.01	54
C6	300.3	110.3	—	—	3.18	21.40	19.76	0.03	0.02	62
C5	280.9	0	—	—	—	20.61	20.26	0.02	0.04	62
C1	248.7	0	—	—	4.10	20.24	11.56	0.06	0.02	68
C3	206.9	0	—	—	2.73	19.26	8.11	0.01	0.01	103

[a] Refer to the time for the projectile to pierce the target, and not to complete perforation (see, e.g. Fig. 6i).

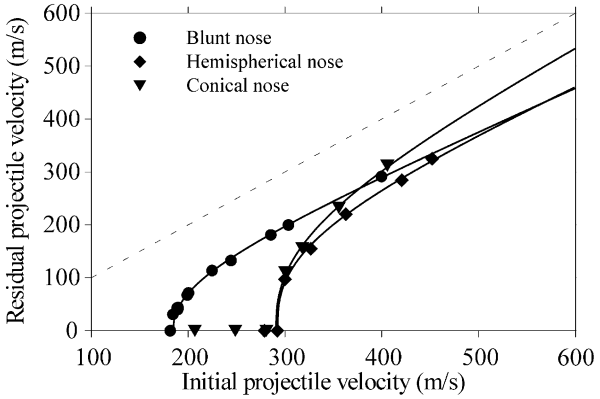

Fig. 3. Residual velocity curves for the different projectile nose shapes.

Table 4
Experimentally obtained ballistic limit velocities and curves

Blunt			Hemispherical			Conical		
v_{bl} (m/s)	a	p	v_{bl} (m/s)	a	p	v_{bl} (m/s)	a	p
184.5	0.79	2.24	292.1	0.81	2.71	290.6	0.95	2.52

residual velocity curves for blunt and hemispherical projectiles seem to coincide as the impact velocity becomes high compared to the respective ballistic limits. The residual velocity curve for conical projectiles exceeds the other two at the highest impact velocities, and becomes almost parallel to the residual velocity line, i.e. the asymptotic response to a target of zero thickness. The residual velocity line is given as the dashed line in Fig. 3. It should be noticed from Table 2 that the projectile deformation in test H7 is high. Post-measurements of the hardness profile of this particular projectile revealed that the core was not as hard as initially specified. Therefore, it might be that the residual velocity curve in Fig. 3 for hemispherical projectiles is somewhat low at the highest impact velocities.

The observed differences in ballistic limit velocities are mainly attributed to the change in failure mode with projectile nose shape. High-speed camera images from typical perforation tests for blunt, hemispherical and conical projectiles are given in Fig. 4. Note that the given times refer to the image taken closest to the assumed time of impact. The images are from tests at an impact velocity close to the ballistic capacity of the target, i.e. approximately 3% above the respective ballistic limits. The figure shows that blunt projectiles cause failure by plugging, and an almost circular plug is ejected from the target. This failure mode is dominated by shear banding. Hemispherical and conical projectiles seem to penetrate the target mainly by ductile hole enlargement, pushing the material in front of the projectile aside. After severe localised bulging, a cup-shaped plug is ejected from the target for hemispherical projectiles. No plug is seen in any of the tests for conical projectiles, but petals are formed on both sides of the cavity. It should be noted that in some of the tests, the projectile rotated during perforation because of an unsymmetrical fracture process, even though the pitch angle prior to impact was measured to be small.

Fig. 5 gives the measured distance–time and velocity–time curves to the projectile based on the digital high-speed camera images from the tests shown in Fig. 4. Significant differences in behaviour during penetration are detected. The blunt projectile shows a sharp drop in velocity after impact, indicating a high interface force between the projectile and target. The slope is far less steep for the other two nose shapes and, in particular, for the conical projectile. Thus, the interface force at impact is reduced accordingly. The perforation time is also seen to increase somewhat both for the hemispherical and conical projectile.

Photographs of the target plates perforated in Fig. 4 are given in Fig. 6(a)–(f). Front surfaces of the targets are shown in Fig. 6(a)–(c), while rear surfaces together with the corresponding projectiles and plugs are shown in Fig. 6(d)–(f). Blunt projectiles cause clean cuts, giving a sharp indentation of the target without any frontal bulge. A modest frontal bulge appears when hemispherical projectiles are used, while a distinct bulge is seen for conical projectiles. In the

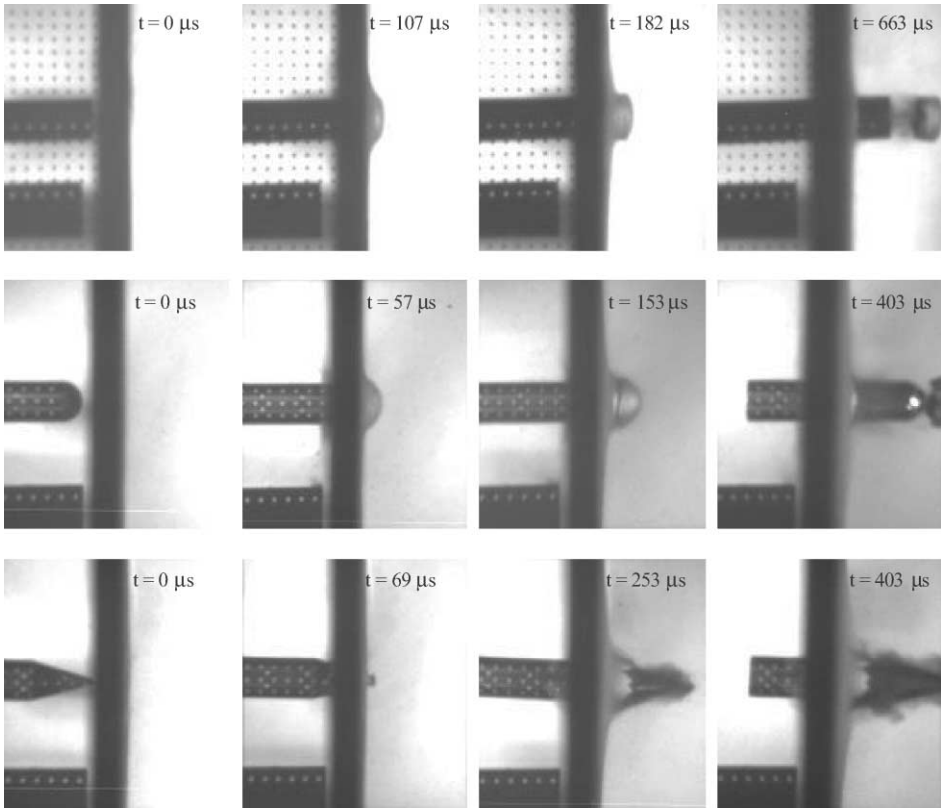

Fig. 4. A selection of high-speed camera images showing perforation of the target plate at impact velocities close to the respective ballistic limits with blunt (Test B15), hemispherical (Test H1) and conical (Test C6) projectiles.

latter, petals are formed because of high circumferential tensile stresses in the bulge. The corresponding rear sides exhibit a somewhat similar behaviour. A modest and smooth bulge is obtained for blunt projectiles, and the punched plug is almost cylindrical with a diameter equal to the nose diameter of the deformed projectile. The bulge for hemispherical projectiles is more irregular and unsymmetrical. The plug is torn out of the target after severe thinning, indicating large tensile forces in the bulge at fracture. As for the frontal side, distinct bulging and petals are obtained for conical projectiles. All cavities in the targets are smooth and uniform, irrespective of the projectile nose shape. As indicated in Tables 1–3, the diameter of the cavity for blunt projectiles is increasing towards the rear side, while for hemispherical and conical projectiles the diameter is reduced. Note also that the rear side diameter of the cavity for hemispherical and conical projectiles is smaller than the initial diameter of the projectile. This indicates considerable elastic deformation and rebound of the target after perforation. Elastic deformations and rebound were also obtained for blunt projectiles, but the effect of these phenomena in the penetration problem is assumed small.

Fig. 6(g)–(i) show some target rear surfaces where complete perforation did not occur. In test H2, a through-thickness-crack was found almost completely around the circumference of the

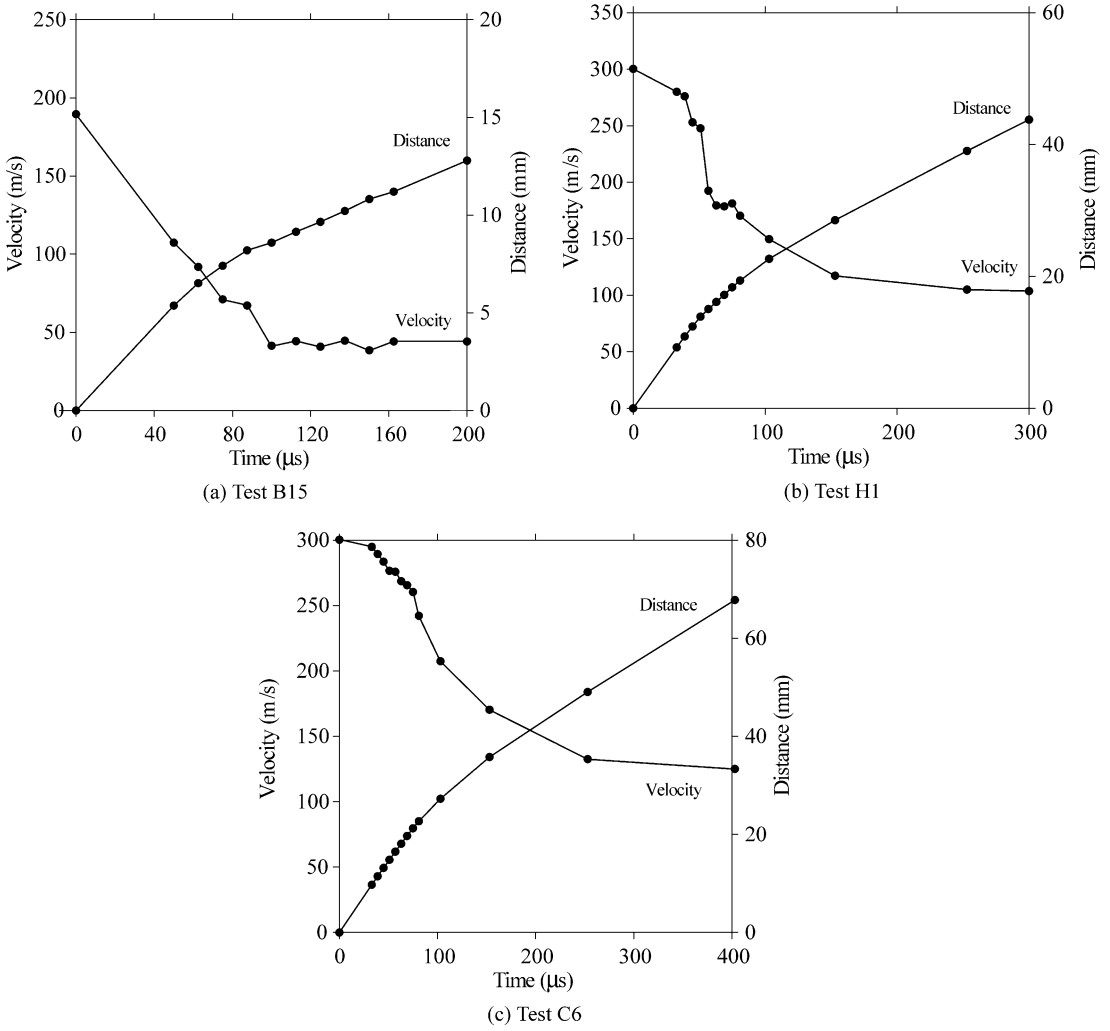

Fig. 5. Measured distance–time and velocity–time curves to the projectile based on the high-speed camera images (some of the images are shown in Fig. 4).

bulge. Test H4 was rather special. Here, the projectile was contained at the tail just before leaving the target, while the plug was fully ejected. This was probably caused by elastic rebound of the target plate, sliding friction between the projectile and target, or by a combination of both. Owing to this behaviour, the impact velocity in test H4 was taken as the ballistic limit of the target for hemispherical projectiles. Conical projectiles easily pierced the target plate, and such failure occurred in all tests reported in Table 3. However, the lowest impact velocities only giving piercing was not taken as the ballistic limit. One example of piercing is shown in Fig. 6(i). Here, only a part of the nose perforated the target, and the projectile was stopped before complete perforation occurred.

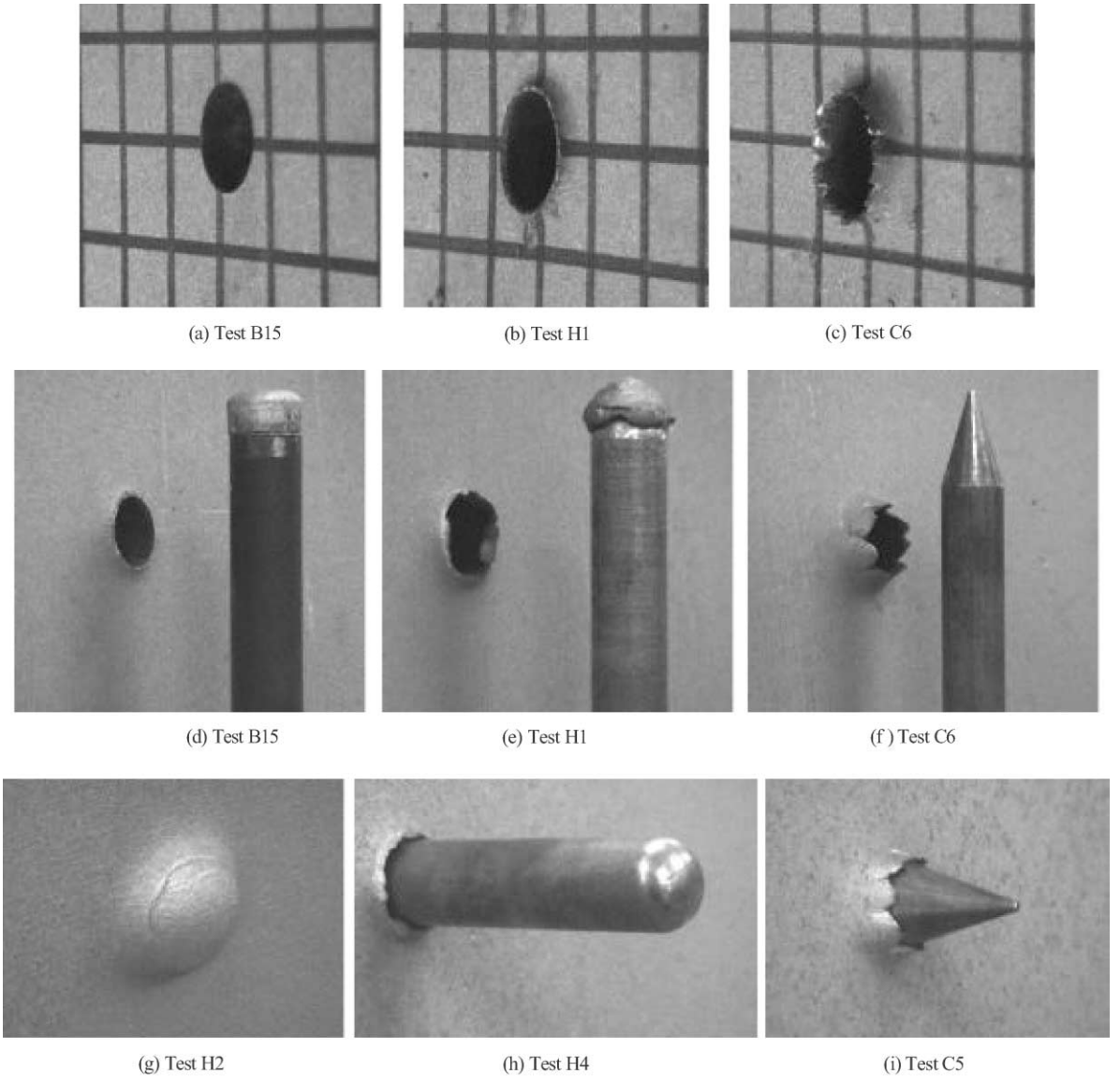

Fig. 6. Details of some targets, projectiles and plugs after the test.

Cross-sections of the target plates perforated in Fig. 4 are shown in Fig. 7. These pictures reveal the differences in plastic flow around the projectile nose during impact. Limited plastic deformation of the target plate seems to appear outside the localised shear zone for blunt projectiles, while the plastic deformation in the vicinity of the penetrating projectile using a conical nose is considerable. In the latter, the moving projectile pushes the material aside radially. This results in a plastic flow field where the material flows either upwards into a frontal bulge or downwards into a rear side bulge, instead of forming a plug. It seems reasonable that more plastic

(a) Test B15 (b) Test H1 (c) Test C6

Fig. 7. Cross-sections of target plates perforated by (a) blunt, (b) hemispherical and (c) conical projectiles.

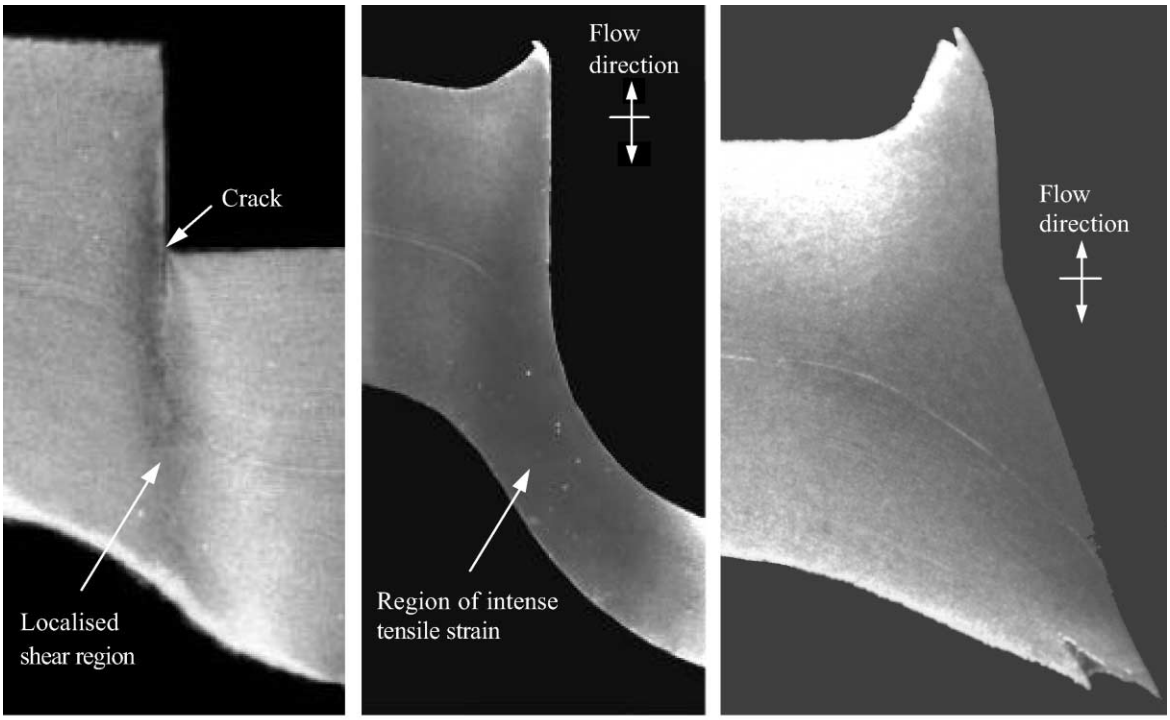

(a) Test B8 (b) Test H2 (c) Test C5

Fig. 8. Macrographs of sectioned and etched target plates close to perforation (not in scale).

work is needed for this operation than to just shear a plug out of the target. The behaviour of hemispherical projectiles seems to be somewhere in between these two extremes.

The plastic flow during the penetration process is further illustrated in the macrographs in Fig. 8 of sectioned and etched cross-sections of target plates close to, but before, complete perforation. When blunt projectiles are used, a sharp and distinct indentation is seen. Due to the high relative velocity between the accelerated material in front of the projectile and the rest of the target, the deformation localises in narrow shear bands. In these localised zones, very large strains, strain rates and temperatures appear, causing material damage. In the present case, the localised deformation is assumed to take place in the transition region between an isothermal and an adiabatic process (see also [16]). Thus, both temperature and damage affect the material

softening. When the strain reaches a critical value, a crack starts to grow towards the rear side of the target, and a plug is finally formed. For hemispherical and conical projectiles the behaviour is different. For the former, the projectile indents the target, giving a very localised bulge and target thinning. The result is regions of intense tensile strain, but no shear localisation. However, as the deformation continues, the material in the intense tensile zone starts to neck. When the tensile strain exceeds the capacity of the target material, a plug with reduced thickness and diameter is ejected. Conical projectiles displace a significant amount of target material radially. The internal separation required for perforation initiates at the tip, and the hole is enlarged along the trajectory of the projectile. Note also that the target deforms to the shape of the conical nose almost perfectly as the projectile indents.

The flow lines of dark pearlite running parallel to the surface of the target as a result of the manufacturing process reveals the plastic flow in the material during penetration. For blunt projectiles these lines are cut straight off and are hardly distorted near the impact surface. As the material in front of the projectile starts to move, the flow lines indicate intense shear inside localised bands, while limited bending is seen outside the bands. Once the deformation localises, the material is constrained to flow in the direction of the moving projectile. Towards the rear side the flow lines are severely stretched, indicating tensile stresses in the bulge. When a hemispherical projectile impacts the target, the flow lines deflect and the material flows up to form a frontal bulge. However, this stage is rapidly overcome and the flow changes direction towards the rear side as the projectile indents the target. The region where the flow lines change direction is indicated in Fig. 8(b). As the indentation continues, the material in front of the projectile stretches and bends, giving parallel and dense flow lines. This results in a region of intense tensile strain, where failure finally is initiated due to necking. In Fig. 8(c), the flow lines indicate that a considerable amount of material flows up and out into a frontal bulge when a conical projectile indents the target, while the material in front and close to the truncated tip flows down and aside. When the nose is completely embedded, the material is just pushed aside by the moving projectile. In the present investigation, the region where the flow lines change direction seems to be close to the middle plane of the target plate. Once this area is passed, the flow lines indicate a downstream movement towards the rear side bulge. The flow pattern is much more complex for conical projectiles than for blunt and hemispherical projectiles.

Fig. 9 gives the measured permanent deformations in projectiles, targets and plugs. As shown in Fig. 9(a), blunt projectiles are rapidly deformed with increasing impact velocity, and at the highest impact velocity a part of the nose of the blunt projectile broke off. The plug thinning is small, again indicating a modest lateral flow of material during plugging. Hemispherical projectiles show limited plastic deformations when the impact velocity is high. The plug thinning is extensive, in agreement with the considerable lateral movement of material during penetration. Conical projectiles hardly deform at all in this velocity regime. Since no plug is formed, the material in front of the projectile is pushed away laterally. The differences in the measured projectile deformation are probably due to the differences in interface force between the projectile and the target, as illustrated in Fig. 5.

The effect on the global target deformation (dishing) for different projectile nose shapes is illustrated in Fig. 9(b)–(d). From Fig. 9(b) the maximum target deformation is seen to decrease from a maximum value at the ballistic limit to a limit value when the impact velocity becomes high. Conical projectiles are found to give the largest global target deformation at all velocities. At

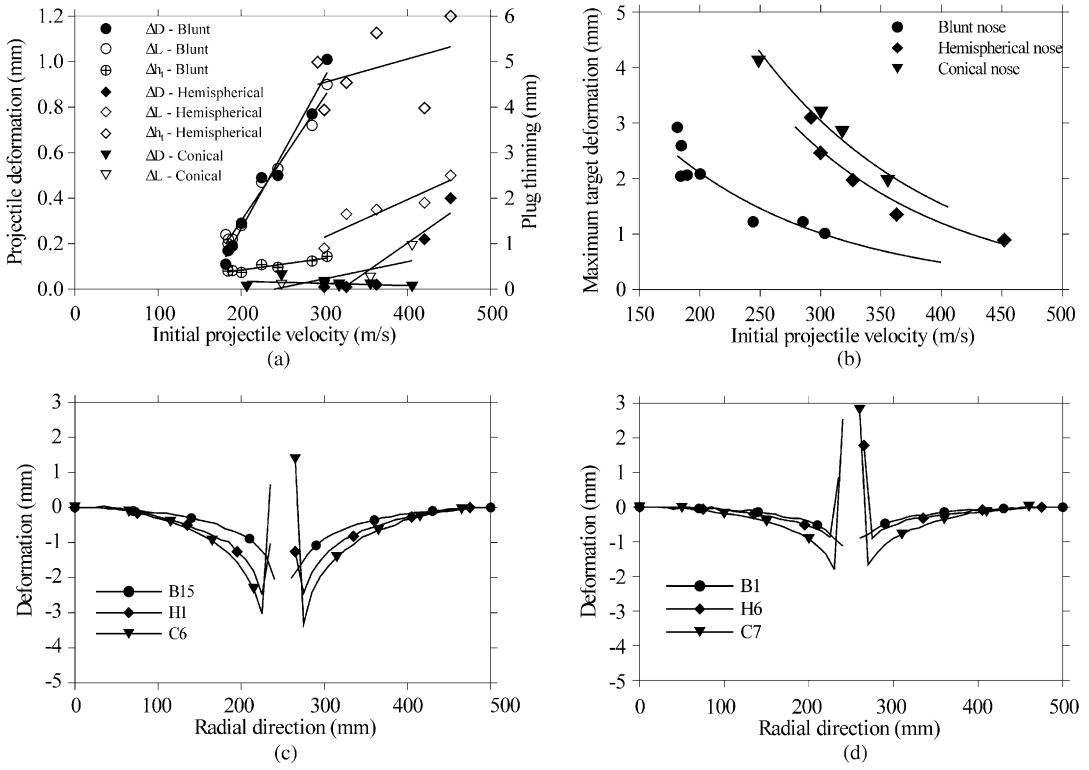

Fig. 9. (a) Projectile deformation and plug thinning versus impact velocity, (b) maximum target deformation versus impact velocity and (c) measured permanent deformation profiles close to the ballistic limit and (d) at the highest impact velocities.

an impact velocity of 300 m/s, the maximum deformation in the target is approximately three times larger for hemispherical and conical projectiles than for blunt projectiles. Note that these measurements do not include the localised bulge. Fig. 9(c) and (d) show comparisons between measured permanent deformation profiles at impact velocities close to and well above the respective ballistic limit velocities. The global target deformation is much more distinct for conical than for blunt projectiles. This is valid also at higher velocities, even if the differences between the deformation profiles are reduced. These measurements also indicate that a larger part of the target plate is activated for conical projectiles than for the other two nose shapes under the given impact conditions.

At impact, the very complex process of transforming projectile kinetic energy into work through a diffuse stress wave transfer begins. In the problem under consideration, it is reasonable to assume that one part of the energy is absorbed in global target deformation (W_g), another part is absorbed in localised plastic flow and failure (W_l), while the rest is absorbed in projectile deformation (W_p). Even if both elastic and frictional work will be done, these are assumed to be of minor importance in the total energy balance during ballistic penetration, and are therefore often neglected [5]. A simple energy balance, where ΔK is the change in the kinetic energy and W is the

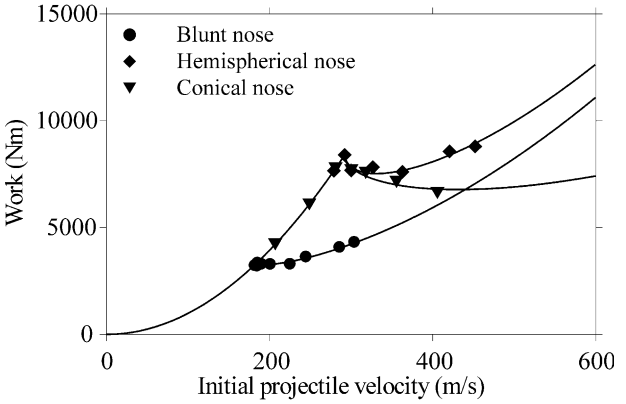

Fig. 10. Measured amount of initial kinetic energy converted into work ($\Delta K = W$) from the tests using different projectile nose shapes.

total work, can then be established as

$$\Delta K = \tfrac{1}{2}m_{\mathrm{p}}v_{\mathrm{i}}^2 - \tfrac{1}{2}m_{\mathrm{p}}v_r^2 - \tfrac{1}{2}m_{\mathrm{pl}}v_{\mathrm{rpl}}^2 = W_{\mathrm{g}} + W_{\mathrm{l}} + W_{\mathrm{p}} = W. \tag{2}$$

The total amount of projectile kinetic energy converted into projectile and target work during impact is easily calculated from the measured values in Tables 1–3, and this is shown in Fig. 10. For blunt projectiles W seems to increase continuously with increasing initial projectile velocity. For conical and hemispherical projectiles W decreases from a local maximum at the ballistic limit to a local minimum, before it again increases monotonically with initial projectile velocity. The drop in W is far less distinct for hemispherical projectiles than for conical projectiles. Blunt projectiles are found to perforate the 12 mm thick Weldox 460 E steel targets with the least energy consumption up to a velocity of approximately 440 m/s. For higher impact velocities, conical projectiles are more efficient. This is partly caused by the difference in projectile plastic deformation (see Tables 1–3) due to the change in interface force and contact surface when the nose shape is varied, as indicated in Figs. 4 and 5. Hemispherical projectiles are found to be the least efficient penetrator in all the tests carried out in this particular study.

However, it is very difficult to quantify the different terms of the work expression in Eq. (2) using simplified computational methods, as also indicated in the literature [2,3]. Woodward [5] showed analytically that for a rigid-plastic material plugging is more favourable than ductile hole enlargement when the target thickness h_{t} is less than $\sqrt{3}D/2$, which in this study gives a target thickness of about 17 mm. In the study by Woodward, only the local area around the projectile nose was considered and the possible effect of adiabatic shear banding was neglected. Bai and Dodd [17] have discussed the mechanisms governing the occurrence and formulation of adiabatic shear bands in detail.

Frictional effects are frequently neglected in impact problems. According to Ravid and Bodner [18] a dynamic friction coefficient of 0.1 is proposed in the literature for metal working operations. A lower value of 0.05 should be used for the lateral surfaces in impact situations due to the higher velocities and temperatures. Recht in Zukas et al. [20] indicated an even lower value. He suggested a dynamic friction coefficient of 0.01 for ballistic impact involving metal to metal surfaces. Fig. 11 shows typical images of the sliding contact area between the target and projectile with a blunt and

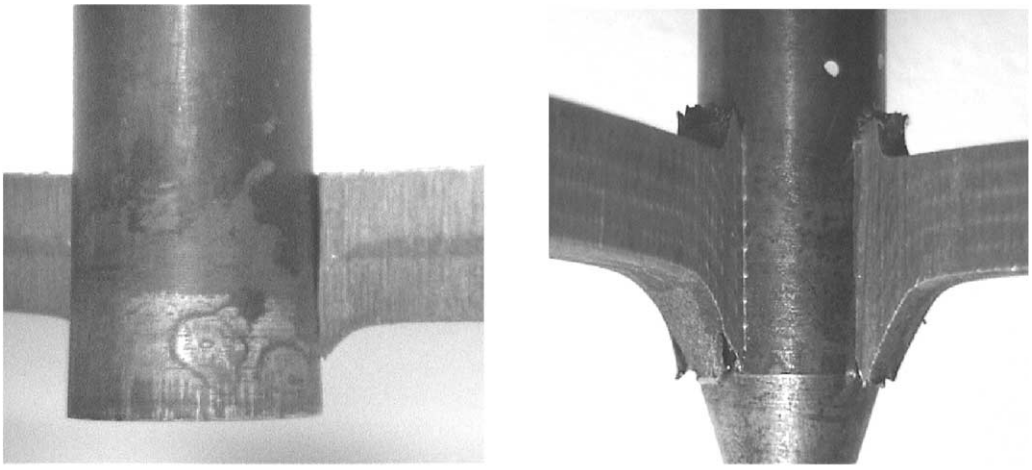

Fig. 11. Sliding contact between projectile and target with (a) blunt (Test B5) and (b) conical (Test C5) nose shape.

a conical nose during penetration. For blunt projectiles the nose becomes plastically deformed at impact, giving it a mushroomed shape, and a plug with a front side diameter almost equal to the deformed nose is formed. The result is a cavity of larger diameter than the initial diameter of the projectile. Thus, after passage of the initial nose the rest of the projectile is hardly in contact with the target (see Fig. 11) and no sliding friction is expected. This is not the case for conical projectiles, where the projectile is in full contact with the target material during the entire penetration and perforation process. Consequently, it seems reasonable to neglect frictional effects for blunt projectiles, while a small frictional coefficient should be used for conical (and hemispherical) projectiles. The minor importance of frictional effects in plate impact with blunt projectiles has previously been validated through numerical simulations [19].

4. Conclusions

This paper presents gas gun experiments in which projectiles with three different nose shapes (blunt, hemispherical and conical) were used to penetrate 12 mm thick Weldox 460 E steel plates. Based on the experimental observations, the following conclusions are drawn:

- The ballistic limit velocity of the target plate is severely affected by the nose shape of the projectile under the given impact conditions. Hemispherical and conical projectiles give a ballistic limit velocity close to 300 m/s, while the ballistic limit velocity is only about 185 m/s for blunt projectiles.
- Also, the residual velocity curves are influenced by projectile nose shape. For blunt and hemispherical projectiles, the residual velocity curves seem to coincide as the impact velocity becomes high compared to the ballistic limit. The residual velocity curve for conical projectiles,

on the other hand, exceeds the other two at the highest impact velocities and becomes almost parallel to the residual velocity line.

- The differences in ballistic limit velocities are attributed to the change in energy absorption and failure mode of the target with projectile nose shape. It appears that both local and global deformations in the target are largest for conical projectiles, followed by hemispherical and blunt projectiles, in that order.
- The variation in the residual velocity curves is partly caused by projectile deformation. Blunt projectiles deform almost linearly with impact velocity in the actual velocity regime, while conical projectiles hardly deform at all. Conical projectiles require less energy to perforate the target plate than the other two projectiles when the impact velocity exceeds 440 m/s. For lower impact velocities, the energy consumption is least for blunt projectiles. Plastic deformations also occur in hemispherical projectiles, but not to the same extent as for the blunt ones.
- From sectioned target plates, it is revealed that sliding frictional effects can be neglected for blunt projectiles. However, small frictional effects seem to be present for conical and hemispherical projectiles, and should be accounted for in finite element simulations.

Acknowledgements

The authors would like to express their gratitude to the Norwegian Defence Construction Service, Central Staff/Technical Division, for their generous financial support of this study.

References

[1] Anderson Jr. CE, Bodner SR. Ballistic impact: the status of analytical and numerical modeling. Int J Impact Eng 1988;7(1):9–35.
[2] Backman ME, Goldsmith W. The mechanics of penetration of projectiles into targets. Int J Eng Sci 1978;16:1–99.
[3] Corbett GG, Reid SR, Johnson W. Impact loading of plates and shells by free-flying projectile. Int J Impact Eng 1996;18(2):141–230.
[4] Baker WE, Westine PS, Dodge FT. Similarity methods in engineering dynamics. In: Theory and practice of scaling modeling, revised ed. Amsterdam: Elsevier, 1991.
[5] Woodward RL. The interrelation of failure modes observed in the penetration of metallic targets. Int J Impact Eng 1984;2(2):121–9.
[6] Zukas JA, et al. Impact dynamics. New York: Krieger Publishing Company, 1992.
[7] Corran RSJ, Shadbolt PJ, Ruiz C. Impact loading of plates—an experimental investigation. Int J Impact Eng 1983;1(1):3–22.
[8] Johnson W, Ghosh SK, Reid S. Piercing and hole-flanging of sheet metals: a survey. Aluminium 1980;56:142–6.
[9] Ipson TW, Recht RF. Ballistic perforation by fragments of arbitrary shape, NWC TP 5927, Denver Research Institute, Naval Weapons Center, China Lake, CA, USA, 1977.
[10] Wingrove AL. The influence of projectile geometry on adiabatic shear and target failure. Metall Trans A 1973;4:1829–33.
[11] Othe S, Yoshizawa H, Chiba N, Shida S. Impact strength of steel plates struck by projectiles. Bulletin JSME 1982;25(205):1226–31.
[12] Wilkins ML. Mechanics of penetration and perforation. Int J Eng Sci 1978;16:793–807.
[13] Børvik T, Langseth M, Hopperstad OS, Malo KA. Perforation of 12 mm thick steel plates by 20 mm diameter projectiles with flat, hemispherical and conical noses, Part II: Numerical simulations, 2001, Int J Impact Eng 2002;27:37–64.

[14] Børvik T, Holen K, Langseth M, Malo KA. An experimental set-up used in Ballistic penetration. In: Jones N, Talaslidis DG, Brebbia CA, Manolis GD (Editors) Proceedings of the fifth international symposium on structures under shock and impact. Thessaloniki, Greece, 1998, 24–26 June. p. 683–92.
[15] Børvik T, Langseth M, Hopperstad OS, Malo KA. Ballistic penetration of steel plates. Int J Impact Eng 1999;22(9–10):855–87.
[16] Børvik T, Leinum JR, Solberg JK, Hopperstad OS, Langseth M. Observations on shear plug formation in Weldox 460 E steel plates impacted by blunt-nosed projectiles. Int J Impact Eng 2001;25(6):553–72.
[17] Bai Y, Dodd B. Adiabatic shear localization: occurrence, theories and applications. Oxford: Pergamon Press, 1992.
[18] Ravid M, Bodner SR. Dynamic perforation of viscoplastic plates by rigid projectiles. Int J Eng Sci 1983;21(6): 577–91.
[19] Børvik T, Hopperstad OS, Berstad T, Langseth M. Numerical simulation of plugging failure in ballistic penetration. Int J Solids Struct 2001;38(34–35):6241–64.
[20] Zukas JA, et al. High Velocity Impact Dynamics. New York: Wiley, 1990.